Two-Photon, ^{13}C and Two-Dimensional ^{1}H NMR Spectroscopic Studies of Retinyl Schiff Bases, Protonated Schiff Bases, and Schiff Base Salts: Evidence for a Protonation Induced $\pi\pi^*$ Excited State Level Ordering Reversal[1]

Robert R. Birge,*[2a] Lionel P. Murray,[2a,b] Raphael Zidovetzki,[2c] and Henry M. Knapp[2a]

Contribution from the Department of Chemistry, Carnegie-Mellon University, Pittsburgh, Pennsylvania 15213, and the Department of Biology, University of California, Riverside, California 92521. *Received June 27, 1986*

Abstract: The $\pi\pi^*$ excited singlet state manifolds of the visual chromophores, *all-trans*-retinylpyrrolidiniminium perchlorate (ATRSBS) and *all-trans-N*-retinylidene-*n*-butylimine:HCl (ATRPSB) are studied by using one-photon and two-photon laser spectroscopy. The goal is a better understanding of how protonation and counterion location affect level ordering in retinyl Schiff bases. Ambient temperature two-photon thermal lensing spectra indicate that ATRSBS has a lowest lying $^{1}A_g{}^{*-}$-like state as was observed previously for *all-trans*-retinal and the Schiff base of *all-trans*-retinal. In contrast, two-photon spectra of ATRPSB indicate that the protonated Schiff base has a lowest lying $^{1}B_u{}^{*+}$-like state. The origin of this level ordering reversal is analyzed by using molecular orbital theory as well as ^{13}C and two-dimensional ^{1}H NMR. We conclude that the relative level ordering of the low-lying "covalent" and "ionic" $\pi\pi^*$ excited states of protonated Schiff bases and Schiff base salts is highly sensitive to counterion location (diffuseness). INDO-PSDCI molecular orbital theory is shown to be a reliable theoretical method of predicting the effect of counterion location on the one-photon and two-photon properties of retinyl protonated Schiff bases and Schiff base salts. This study provides further experimental support for the conclusions of a previous two-photon investigation of the rhodopsin binding site which demonstrated that the protein bound 11-*cis*-retinyl chromophore is protonated and occupies a neutral binding site.

I. Introduction

Although the nature of the chromophore binding site of rhodopsin remains a subject of debate, a majority of researchers now believe that the retinyl chromophore, 11-*cis*-retinal, is bound to the opsin protein via a protonated Schiff base linkage.[3-15] In order to understand the photophysical origins of the unusually rapid (<3 ps), high quantum yield (0.67) primary photochemical event of rhodopsin, the effect of protonation on the excited state level ordering and the photochemical properties of the chromophore must be understood. Two-photon excitation studies indicate that both *all-trans*-retinal (ATR) and its Schiff base (ATRSB) (Figure 1) have lowest lying $^{1}A_g{}^{*-}$-like states.[15-17] More recently, two-photon thermal lens spectroscopy has shown that incorporation of 11-*cis*-retinal into the binding site of rhodopsin induces a level ordering reversal, i.e., a lowest lying $^{1}B_u{}^{*+}$-like state.[15,18] The model chromophore studies presented in this paper have as their goal a better understanding of the origin and photophysical consequences of this latter observation.

Previous theoretical studies have suggested that protonation of the Schiff base induces a level ordering reversal and that the combination of a fixed counterion and a lowest lying $^{1}B_u{}^{*+}$-like state is responsible for a barrierless excited state potential surface for 11-cis ↔ 11-trans isomerization.[19-21] These predictions have not received universal acceptance, however. Palmer et al. carried out spectroscopic studies of a dodecapentaenylidene-*n*-butylamine Schiff base and concluded that protonation does not induce a level ordering reversal.[22] A detailed study of the photochemistry of a variety of model visual chromophores by Becker and Freedman led these authors to conclude that level mixing, rather than level ordering reversal, is the key photophysical event responsible for efficient photoisomerization.[23] The studies reported in this paper will partially resolve the issues raised in the above two investigations.

The two model chromophores spectroscopically and theoretically studied in this paper have been used frequently by investigators as models of the protein bound chromophore of rhodopsin.[5,13,23] *all-trans-N*-Retinylidene-*n*-butylimine:HCl (ATRPSB, Figure 1) provides a good model for the chromophore in rhodopsin because the protonated *n*-butylamine moiety provides an analogous covalent linkage as that afforded by the ϵ-lysine group of opsin.[13] The *all-trans*-retinylpyrrolidiniminium perchlorate salt (ATRSBS, Figure 1) is a less realistic model in terms of chromophore

(1) Abstracted in part from the Ph.D. Thesis of L. P. Murray, Carnegie-Mellon University, 1985.
(2) (a) Carnegie-Mellon University. (b) Permanent address: Laboratory of Chemical Physics, National Institute of Arthritis, Diabetes, and Kidney Diseases, Bethesda, MD 20892. (c) University of California, Riverside.
(3) Birge, R. R. *Ann. Rev. Biophys. Bioeng.* **1981**, *10*, 315.
(4) Honig, B. In *Biological Events Probed by Ultrafast Laser Spectroscopy*; Alfano, R. R., Ed.; Academic Press: New York, 1982; pp 281-297.
(5) (a) Irving, C. S.; Byers, G. W.; Leermakers, P. A. *Biochemistry* **1970**, *9*, 858. (b) Irving, C. S.; Byers, G. W.; Leermakers, P. A. *J. Am. Chem. Soc.* **1969**, *91*, 2141.
(6) Kliger, D. S. *Int. J. Quantum Chem.* **1979**, *16*, 809.
(7) Kohler, B. E. *Biophys. Struct. Mech.* **1977**, *3*, 101.
(8) Mathies, R. In *Chemical and Biological Applications of Lasers*; Moore, C. B., Ed.; Academic Press: New York, 1979; pp 55-99.
(9) Oseroff, A. R.; Callender, R. H. *Biochemistry* **1974**, *13*, 4243.
(10) (a) Ottolenghi, M. *Adv. Photochem.* **1980**, *12*, 97. (b) Ottolenghi, M. *Methods Enzymol.* **1982**, *88*, 470.
(11) (a) Sheves, M.; Nakanishi, K. *J. Am. Chem. Soc.* **1983**, *105*, 4033. (b) Sheves, M.; Nakanishi, K.; Honig, B. *J. Am. Chem. Soc.* **1979**, *101*, 7086.
(12) Tavan, P.; Schulten, K.; Oesterhelt, D. *Biophys. J.* **1985**, *47*, 415.
(13) (a) Waddell, W. H.; Becker, R. S. *J. Am. Chem. Soc.* **1971**, *93*, 3788. (b) Waddell, W. H.; Schaffer, A. M.; Becker, R. S. *J. Am. Chem. Soc.* **1973**, *95*, 8223. (c) Waddell, W. H.; Schaffer, A. M.; Becker, R. S. *J. Am. Chem. Soc.* **1977**, *99*, 8456.
(14) Warshel, A.; Barboy, N. *J. Am. Chem. Soc.* **1982**, *104*, 1469.
(15) Birge, R. R. *Acc. Chem. Res.* **1986**, *19*, 138.
(16) Birge, R. R.; Bennett, J. A.; Hubbard, L. M.; Fang, H. L.; Pierce, B. M.; Kliger, D. S.; Leroi, G. E. *J. Am. Chem. Soc.* **1982**, *104*, 2519.
(17) Murray, L. P.; Birge, R. R. *Can. J. Chem.* **1985**, *63*, 1967.
(18) Birge, R. R.; Murray, L. P.; Pierce, B. M.; Akita, H.; Balogh-Nair, V.; Findsen, L. A.; Nakanishi, K. *Proc. Natl. Acad. Sci. U.S.A.* **1985**, *82*, 4117.
(19) Birge, R. R.; Hubbard, L. M. *J. Am. Chem. Soc.* **1980**, *102*, 2195.
(20) Birge, R. R.; Hubbard, L. M. *Biophys. J.* **1981**, *34*, 517.
(21) Birge, R. R. In *Biological Events Probed by Ultrafast Laser Spectroscopy*; Alfano, R. R., Ed.; Academic Press: New York, 1982; pp 299-317.
(22) Palmer, B.; Jumper, B.; Hagan, W.; Baum, J. C.; Christensen, R. L. *J. Am. Chem. Soc.* **1982**, *104*, 6907.
(23) Becker, R. S.; Freedman, K. *J. Am. Chem. Soc.* **1985**, *107*, 1477.

0002-7863/87/1509-2090$01.50/0

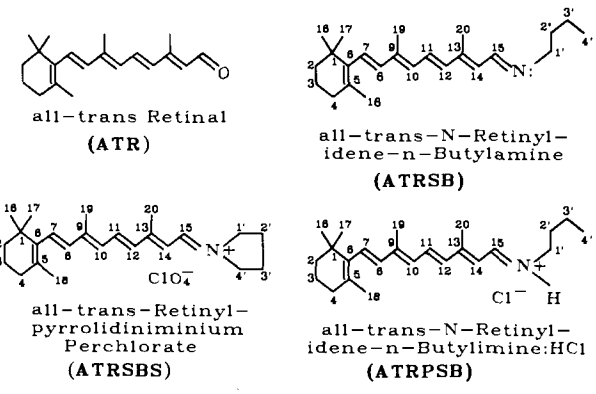

Figure 1. Structures of the four *all-trans*-retinyl polyenes analyzed in this paper. Abbreviations used to identify these polyenes are indicated in bold face underneath the formal names. The carbon atom numbering scheme is also shown for ATRSB, ATRPSB, and ATRSBS.

structure, but its (one-photon) spectroscopic similarities, more diffuse counterion, and comparative stability in a variety of solvents, make it a valuable model chromophore.[5,24] Indeed, although we will demonstrate below that ATRSBS has a different excited state $\pi\pi^*$ level ordering than that observed for ATRPSB (or the chromophore in rhodopsin), our ability to resolve the origin of this level ordering reversal provides new insights into how the protein regulates the photophysical properties of the opsin bound chromophore.

II. Experimental Section

Sample Preparation. *all-trans*-Retinylpyrrolidiniminium perchlorate (ATRSBS) was prepared by method A of Leonard and Paukstelis[24] with a few variations. A stoppered 25-mL, round-bottomed flask containing 1.00 g (3.52 mmol) of *all-trans*-retinal (Eastman-Kodak, lot no. C12A), 0.66 g (3.85 mmol) of pyrrolidine perchlorate, 3Å molecular sieves, and a stir bar under an atmosphere of dry nitrogen was placed in an ice bath. Freshly distilled high purity ethanol (5–10 mL) was added to the reaction vessel with a Millipore filtration-syringe assembly (Fluoropore 0.2 μm). Dark crystals formed throughout the deep red solution upon stirring for 6 h in the dark or under red lights. The crystals were collected onto a Büchner funnel and washed with room temperature isopropanol to remove unreacted pyrrolidine perchlorate. The dark powder was then washed with anhydrous diethyl ether until the washings were no longer yellow due to unreacted *all-trans*-retinal. This yielded a fine black powder of ATRSBS. The Büchner funnel was covered with filter paper in order to air dry the sample (approximately 10–15 min). The powder was then washed with diethyl ether, air dried, and stored in a vacuum desiccator. NMR spectroscopy verified that the ATRSBS sample was free of rotational isomers (see below), and visible absorption spectra agreed with those published.[5] The reagents pyrrolidine and perchloric acid were obtained from Aldrich and Mallinckrodt, respectively, while the absolute ethanol was from Gold Shield.

all-trans-N-Retinylidene-*n*-butylimine:HCl (ATRPSB) was made by the method of Palmer et al.[22] The precursor, *all-trans-N*-retinylidene-*n*-butylimine (ATRSB), was made by reacting *all-trans*-retinal (ATR) under nitrogen in freshly distilled *n*-butylamine (Aldrich) in the presence of 3Å molecular sieves at 0 °C for 6 h. The *n*-butylamine was added in molar excess (50:1) and then removed by rotary evaporation upon completion of the reaction [as monitored with a Varian Cary 17D UV–vis spectrophotometer and by reverse-phase thin-layer chromatography (solvent: acetonitrile)]. Small portions of carbon tetrachloride were added to the sample for rotary evaporation to ensure complete removal of excess *n*-butylamine. ATRPSB was made in situ by bubbling HCl gas (Matheson, Technical grade, dried with H_2SO_4, silica gel, and $CaCl_2$) into the solution within the sample cells prior to spectral measurements.[13b] Careful drying is essential, even when using an ATRPSB filtrate produced by Blatz's method,[25] to prevent reformation of the Schiff base of retinal.

Isomeric purity of the *all-trans*-retinyl polyenes was verified to be >95% with ^1H and ^{13}C NMR spectroscopy (see section IV.D.).

One-photon absorption spectra were taken with a Varian Cary 17D spectrophotometer. An optical Dewar assembly filled with liquid nitrogen was used in the nitrogen purged sample chamber to take the low-temperature (77 K) spectra.[26]

Uncorrected emission spectra were taken with a variable temperature emission apparatus at 77 K. A 100-W mercury lamp (Illumination Industries, model LH351Q) filtered by using a 440-nm interference filter (SBW = 5 nm) was used as the excitation source. A 3-cm focal length lens was used to focus the 440-nm excitation into the quartz sample cell (3.8 mm ID) at the cold tip of a closed cycle helium refrigeration system (Air Products, Displex model CS-202 equipped with a model APD-E temperature controller). The temperature controller was equipped with a Chromel/Gold thermocouple to monitor the temperature of the sample at the tip of the He expander module. The resulting fluorescence was monitored at 90° to the excitation source with a computer controlled GCA/McPherson grating monochromator[26] (Model EU-700-56, slit width: 350 μ for ATRSBS, 1700 μ for ATRPSB). A cooled [Pacific Photometric Model 3461 along with a Model 33 temperature controller and a Neslab RTE-8 refrigeration system (5 °C)] photomultiplier tube (Hamamatsu R955, 800 V) was used to detect the fluorescence. The photomultiplier output was connected to a picoammeter (Keithley, Model 414A), and a PDP 11/03 was used for signal processing.

Two-photon thermal lensing spectra were taken by using the spectrometer shown in Figure 2. We adopted the thermal lensing method rather than the excitation method because of the low fluorescence quantum yields of ATRSBS and ATRPSB. The wavelengths of laser excitation for ATRSBS ranged from 750 nm to 990 nm, while for ATRPSB the spectra were obtained from 660 nm to 980 nm. The thermal lensing signal was amplified with a Model 113 preamplifier prior to measurement with a Model 165 gated integrator and a Model 162 boxcar averager (EG&G Princeton Applied Research). All other aspects of data collection were as described previously in ref 18.

Nuclear magnetic resonance spectra were recorded on a Bruker WM 500 spectrometer, operating at a magnetic field of 11.74 Tesla, ^1H frequency of 500.13 MHz, and ^{13}C frequency of 125.767 MHz. Chromophore concentrations of 0.01 M were used in Me_2SO-d_6 or $CDCl_3$, and the spectra were taken by using 5- or 10-mm tubes. The solvent was used for a field frequency lock, and Me_4Si was used as an internal standard.

^{13}C NMR. Most of the ^{13}C NMR spectra were taken with broad band proton decoupling and NOE. Typically, 3-s relaxation delay with a 40° pulse was employed. The assignment of the peaks was made by using proton-coupled ^{13}C NMR, making measurements without NOE, and by using the previously published data on related compounds.[27–29]

One-dimensional ^1H NMR spectra were acquired in the quadrature-phase detection mode with 16 or 32 K data points, 60° pulse width, a cycling time between scans of 2 s, and a spectral width of 6000 Hz. Some spectra were resolution enhanced by using a Gaussian multiplication routine which multiplied the free induction decay (FID) with a Gaussian centered at 18–21% of the total decay time and a negative line broadening ranging from −1.8 to −2.5 Hz.

Two-dimensional ^1H-NMR spectroscopy utilized scalar *J*-correlation spectroscopy (COSY) to obtain ^1H–^1H *J*-connectivity maps. The COSY spectra were recorded with a sequence of two nonselective 90° pulses[30] $(90°\text{-}t_1\text{-}90°\text{-}t_2)_n$. The recycle delay was 2 s, and a 2 K square data matrix was accumulated. A 16-phase cycling was used for each t_1 to reduce spectral distortions. The phase sequence was introduced by Dr. L. Mueller (now at Smith-Klein & Beckman, Philadelphia) and is available from the authors on request. Prior to Fourier transformation, the matrix was multiplied along the F1 dimension by a sine bell squared function and along the F2 dimension by a sine bell function. The assignment of the proton resonances of ATRSBS was done through analysis of the COSY spectrum, consideration of ^1H–^1H splitting patterns and coupling constants obtained from the one-dimensional spectrum, and comparison with published spectra of related compounds (see section IV.D.).

Spectroscopic Solvents. The following spectral solvents were used in our studies: EPA (diethyl ether:isopentane:ethyl alcohol, 5:5:2), 2-methyltetrahydrofuran (2M THF), carbon tetrachloride (Mallinckrodt, Spectra), and Me_2SO-d_6 (99.9 atom D, Aldrich, gold label). The ethanol (Gold Shield, absolute) was freshly distilled over magnesium shavings and iodine in an inert atmosphere. The diethyl ether (Burdick and Jackson, without ethanol preservative), isopentane (Aldrich, 2-methylbutane, gold label), carbon tetrachloride, and Me_2SO (spectrograde) were used as

(24) Leonard, N. J.; Paukstelis, J. V. *J. Org. Chem.* **1963**, *28*, 3021.
(25) Blatz, P. E.; Mohler, J. H.; Navangal, H. V. *Biochemistry* **1972**, *11*, 848.
(26) Birge, R. R. In *Ultrasensitive Laser Spectroscopy*; Kliger, D. S., Ed.; Academic Press: New York, 1983; pp 109-174.
(27) Shriver, J. W.; Mateescu, G. D.; Abrahamson, E. W. *Biochemistry* **1979**, *18*, 4785.
(28) Shriver, J. W.; Abrahamson, E. W.; Mateescu, G. D. *J. Am. Chem. Soc.* **1976**, *98*, 2407.
(29) Pattaroni, C.; Lauterwein, T. *Helv. Chim. Acta.* **1981**, *64*, 1969.
(30) Aue, W. P.; Bartholdi, E.; Ernst, R. R. *J. Chem. Phys.* **1976**, *64*, 2229.

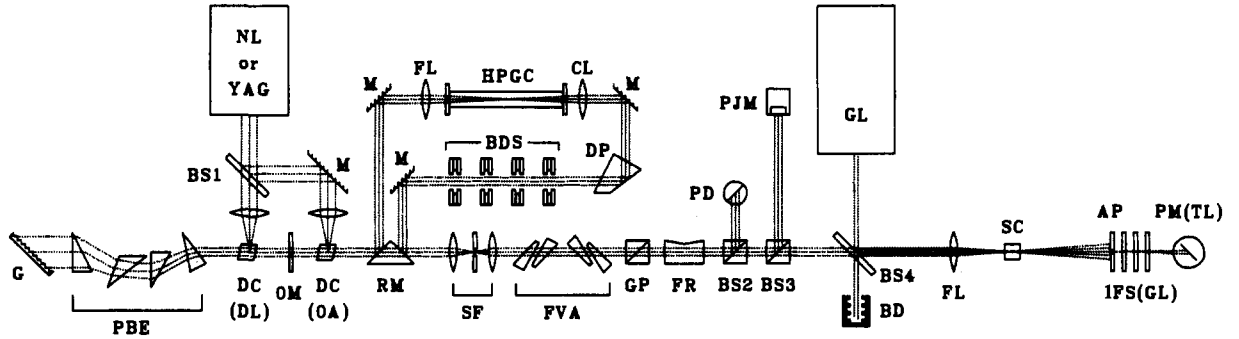

Figure 2. Schematic diagram of the two-photon thermal lens spectrometer used in the present investigation of ATRSBS and ATRPSB. A 900 KW nitrogen laser (NL) or the first or second harmonic of a ND-YAG laser (YAG) is used to simultaneously pump two dye cells (DC) to produce optically amplified tunable dye laser excitation. A spatial filter (SF) is used to select TEM_{00}, and a Fresnel wedge variable attenuater (FVA) is used to adjust the intensity of the laser beam. The Fresnel rhomb (FR) produces circularly polarized light or linearly polarized light depending upon angle of rotation. Two beam splitters (BS2 and BS3) direct a small fraction of the laser excitation onto a photodiode (PD) to measure pulse width and a pyroelectric Joule meter (PJM) to measure pulse energy. The thermal lens spectra are obtained by using a beam splitter (BS4) to combine the output of a continuous HeNe wave gas laser (GL) with the pulsed laser output to provide a collinear beam. The beam is then focused slightly in front of the sample cell (SC) by using an achromatic focusing lens (FL). A small diameter aperture (AP) passes a small fraction of laser light through three interference filters (IFS(GL)) with band passes at 632.8 nm (the wavelength maximum of the HeNe laser). A thermal lens signal is collected by using a photomultiplier (PM(TL)) connected to a box car averager with time delayed baseline sampling capability (EG&G PAR 165/162).

Table I. Franck–Condon One-Photon and Two-Photon Maxima and Stokes Shifts in Various Visual Chromophores in Solution[a]

molecule[b]	solvent	$\Delta\bar{\nu}(B \leftarrow S_0)$[c]	$\Delta\bar{\nu}(A \leftarrow S_0)$[d]	$\Delta\bar{\nu}(S_1 \rightarrow S_0)$[e]	$\Delta\Delta\bar{\nu}(B-A)$[f]	$\Delta\Delta\bar{\nu}(B-F)$[g]	$\Delta\Delta\bar{\nu}(A-F)$[h]	$\int B \cdot Fd\bar{\nu}/\int Fd\bar{\nu}$[i]
ATR	EPA (77 K)	25.8	23.4	19.1, 18.3	2.4	~7.1	~4.7	<0.01
ATRSB	EPA (77 K)	26.5	23.7	19.2, 17.8	2.8	~8.0	~5.2	<0.01
ATRSBS	EPA (77 K)	22.7, 24.5		16.2		~7.4		~0.02
ATRSBS	2M THF	22.1[j]	21.6[j]	16.6[k]	0.5[j]	5.7[k]	5.0	~0.02[k]
ATRPSB	2M THF, CCl_4	22.8[k]	23.4[l]	18.0[k]	−0.6[l]	4.8[k]	5.4	~0.12[k]

[a] All spectral data are in wavenumbers × 10^{-3}. If two values are given, there are two vibronic maxima of nearly equal intensity. Under these cases, the $\Delta\Delta\bar{\nu}$ values are calculated by averaging the positions of the vibronic maxima. Data for ATR and ATRSB from ref 16 and 17, respectively. [b] See Figure 1. [c] One-photon absorption maxima of the "$^1B_u^{*+}$" ← S_0 transition. [d] Two-photon excitation or thermal lens maximum of the "A_g^{*-}" ← S_0 transition. [e] Vibronic maxima of fluorescence spectra. [f] Franck–Condon splitting of the "$^1B_u^{*+}$" minus the "$^1A_g^{*-}$" state maxima. The spectroscopic splitting underestimates the energy separation of the $^1A_g^{*-}$-like and $^1B_u^{*+}$-like states in ATRSBS and ATRPSB because of significant intrastate mixing of one-photon and two-photon allowedness. [g] Stokes shift of the fluorescence and one-photon maxima. [h] Stokes shift of the fluorescence and two-photon maxima. [i] Area of spectral overlap of normalized one-photon absorption spectrum and normalized fluorescence spectrum divided by total area of normalized fluorescence spectrum. [j] Data for 2M THF at ~22 °C. The one-photon absorption maximum red shifts approximately 250 cm^{-1} upon lowering the temperature to 77 K. [k] 2M THF (77 K) [l] CCl_4 room temperature.

purchased. The solvents EPA and 2M THF were filtered and dried (Fluoropore filters, 0.2 μm pore size) by passing each through a Millipore syringe assembly. The solvent was then injected into a septum covered volumetric flask containing a preweighed amount of sample (ATRSBS or ATRPSB) in an atmosphere of nitrogen. Concentrations of ~10^{-5} M were used for the absorption spectra. The optical density at λ_{max} of samples used to obtain the fluorescence spectra was adjusted to <0.8 to minimize self-absorption. Concentrations of ~10^{-3} M were used for the two-photon investigations.

III. Theoretical

The molecular orbital calculations used the all-valence electron semiempirical INDO-PSDCI procedures described in ref 16, 19, and 20. All single excitations below 15 eV and all double excitations below 20 eV were included in the CI Hamiltonian for the excited-state calculations. These energy constraints normally result in a CI Hamiltonian containing ~150 single and ~325 double excitations for the molecules investigated in this paper. Ground-state calculations used to calculate the energy of the total chromophore–counterion system as a function of counterion location did not include configuration interaction. Test calculations indicated that the introduction of double CI did not alter qualitatively the assignment of counterion location.

The effect of solvent environment on the ground-state energy of the chromophore–counterion system was calculated approximately by using the free energy relationships associated with solute–solvent dipole–dipole interactions from ref 33 (eq 8 and 9). In order to simulate a highly polar solvent environment, the dielectric constant of the solvent was assigned an unrealistically high number (ϵ = 150) to partially compensate for the fact that hydrogen bonding effects were not included. The solute cavity radius was assigned to be 2.5 Å, and the dipole moment of the chromophore–counterion system was calculated by using INDO molecular orbital theory (see above). The cavity radius was assigned based on the assumption that the vast majority of the electrostatic energy is concentrated in the region of the counterion and the 6 carbon segment lying nearest to the counterion.

Two-photon absorptivities were calculated by using the methods and procedures described in ref 34. Calculations were carried out including and excluding the contribution of the initial and final states to the two-photon absorptivity for comparison. Although the contribution of the initial and final states should be formally included (see discussion in ref 34), the use of semiempirical molecular orbital methods and the neglect of solvent occasionally leads to calculated absorptivities that are less accurate than those calculated neglecting these terms (see discussion in ref 16). The origin of this problem lies in the extreme sensitivity of the two-photon absorptivity to dipole moment changes upon excitation, and the neglect of solvent reaction field to the total dipole moment can lead to large error. ATRPSB and ATRSBS have very large calculated ground-state dipole moments (μ = 24.4 D, Figure 5a; μ = 22.6 D, Figure 5b; μ = 16.8 D, Figure 5c). These values, coupled with large changes in dipole moment upon excitation, yield calculated two-photon absorptivities that often exceed 10^{-48} cm^4 s $molecule^{-1}$ $photon^{-1}$ when initial and final states are included. Accordingly, we will limit our discussion of calculated two-photon absorptivities to qualitative comparisons of relative allowedness. In general, the absorptivities relate inversely to the one-photon oscillator strength.

IV. Results and Discussion

A. Optical Spectroscopy. One-Photon Spectroscopy. One-photon absorption and one-photon-induced fluorescence spectra of ATRSBS and ATRPSB are shown in Figure 3. The analysis of the one-photon data is presented in Table I. It is interesting to note that the absorption spectra are invariably broad and structureless, but that the fluorescence spectra display a modest

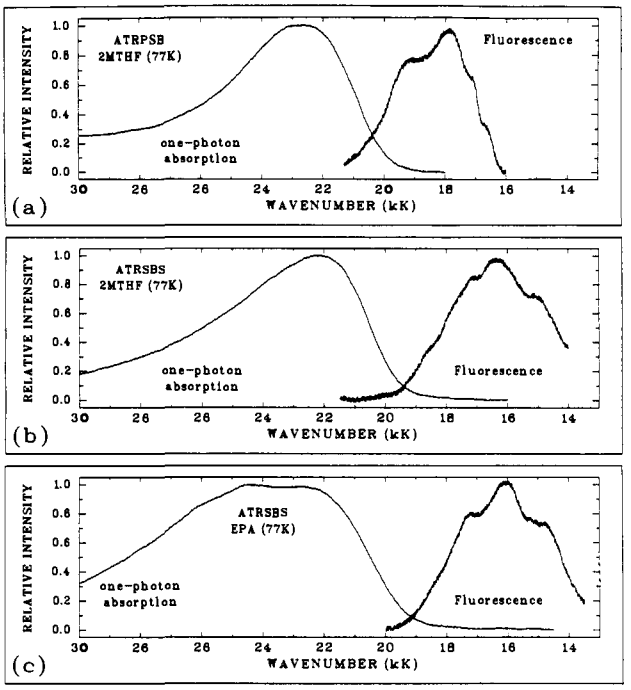

Figure 3. One-photon absorption and one-photon induced fluorescence spectra of ATRPSB and ATRSBS in 77 K glasses. The spectra of ATRPSB were taken in 2-methyltetrahydrofuran (a). The spectra of ATRSBS were taken in two solvents, 2-methyltetrahydrofuran (b) and the solvent mixture EPA (c).

amount of vibronic structure in both polar and nonpolar solvent. This observation suggests that at least two excited singlet states contribute intensity to the λ_{max} absorption band. This prediction is supported by the molecular orbital calculations which indicate that both the low-lying $^1A_g{}^{*-}$-like and $^1B_u{}^{*+}$-like states have (one-photon) oscillator strengths >0.3. Of equal significance is the observation that the normalized overlap between the fluorescence and absorption spectra is much larger in ATRPSB (normalized overlap $\simeq$ 0.12, see Table I) than in ATR, ATRSB, or ATRSBS. Although Franck–Condon factors (i.e., large changes in geometry upon excitation) can be responsible for producing very small normalized overlaps, small overlaps in the case of polyenes are normally the result of two low-lying singlet states, the higher (allowed) singlet responsible for the λ_{max} absorption band, and the lowest lying singlet (with a significantly lower oscillator strength) responsible for the fluorescence spectrum. The observation that ATRPSB has a significantly larger normalized overlap between absorption and fluorescence suggests, but does not prove, that the excited state responsible for the λ_{max} absorption band is also the lowest lying, fluorescing singlet state. The smaller Franck–Condon–Stokes shift between absorption and fluorescence maxima in ATRPSB (4800 cm^{-1}) relative to the other polyenes (see Table I) supports this observation.

The effect of solvent environment upon the absorption and fluorescence spectra of ATRSBS is demonstrated in Figure 3 (parts b and c). The absorption spectrum of ATRSBS in polar (EPA) solvent is significantly broadened, but the fluorescence spectrum is affected only slightly by increasing solvent polarity. This observation supports further the prediction that at least two excited singlet states are responsible for the broad λ_{max} absorption band and implies that the higher energy state has a larger oscillator strength.

Two-Photon Spectroscopy. ATRSBS and ATRPSB exhibit very low quantum yields of fluorescence at both ambient and reduced temperatures (77 K) ($\Phi_f < 0.1$).[13,35] Accordingly, the two-photon excitation technique[26] is inherently less sensitive than the thermal lens method[15,18,30,31] for observing the two-photon spectrum. A further advantage of adopting the thermal lens method is that the two-photon spectra can be observed by using ambient temperature solutions, which allows for higher solute concentrations and improves the signal-to-noise ratio of the spectra. Unfortunately, we were unable to find a suitable ambient temperature solvent that could be used for both ATRSBS and ATRPSB and simultaneously did not have an overtone one-photon absorption spectrum that interfered with the two-photon thermal lens spectrum of the sample. The one-photon absorption and two-photon thermal lens spectra of ATRPSB in CCl_4 and of ATRSBS in 2M THF are shown in Figure 4, along with the one-photon absorption and fluorescence spectra taken in 2M THF at 77 K. Analysis of the spectra indicates that the use of different solvents for collecting the two-photon spectra does not cause ambiguities due to solvent-induced shifts of the Franck–Condon maxima. In other words, intrinsic electronic properties rather than solvent effects are responsible for the differences in excited level ordering between ATRSBS and ATRPSB.

The two-photon thermal lens maximum of ATRSBS is observed $\sim$500 cm^{-1} below the one-photon Franck–Condon maximum (Figure 4b). In contrast, the two-photon thermal lens maximum of ATRPSB lies $\sim$600 cm^{-1} above the one-photon Franck–Condon maximum (Figure 4a). The theoretical calculations described below provide support for the simple interpretation that the above differences in one- and two-photon FC maxima signal a level ordering reversal between ATRPSB and ATRSBS. In particular, ATRSBS has a lowest lying $^1A_g{}^{*-}$-like state as was observed in ATR[16] and ATRSB.[17] Analysis of the two-photon data indicate that ATRPSB has a lowest lying $^1B_u{}^{*+}$-like state, as was observed for the protein-bound chromophore of rhodopsin.[18] The fact that the one-photon absorption maximum and the two-photon thermal lens maximum are so close in energy does not indicate that the system origins of the $^1A_g{}^{*-}$-like and $^1B_u{}^{*+}$-like states lie within $\sim$500 cm^{-1}. Rather, the close proximity of the maxima indicates the very strong mixing of *g* and *u* character associated with the high polarity of ATRSBS and ATRPSB. Accordingly, it is important to emphasize the approximate nature of the symmetry labels. Both $^1A_g{}^{*-}$-like and $^1B_u{}^{*+}$-like states contribute to the one-photon absorption as well as the two-photon thermal lens vibronic distributions. This qualitative observation will be evaluated in more detail by using molecular orbital theory.

B. Molecular Orbital Calculations. All-valence electron semiempirical INDO molecular orbital theory was used to calculate equilibrium counterion–chromophore conformations, and INDO-PSDCI theory was used to calculate the resultant one-photon and two-photon properties (see section III). The results are shown in Figure 5–7. Although the effect of solvent was introduced in an approximate way in evaluating the two counterion potential surfaces shown in Figure 7, the molecular orbital calculations in all other respects neglected solvent effects. Accordingly, the assumption of "vacuum conditions" implicit in these calculations must be recognized and the results interpreted with caution since solvent can play a crucial role in stabilizing highly polar compounds.

ATRPSB. The molecular orbital calculations indicate that the counterion location shown in Figure 5a is the most stable geometry for ATRPSB. A strong hydrogen bond is formed between the imine proton and the Cl^- atom, and the presence of this hydrogen bond is confirmed in the proton NMR spectra.[28] INDO-PSDCI calculations of the excited level ordering of ATRPSB are compared to the experimental FC maxima in Figure 6. Calculated one-photon oscillator strengths are shown above the rectangles used to indicate the transition maxima. Calculated two-photon absorptivities inversely mirror the one-photon oscillator strengths. Although the calculations underestimate the transition energies, it is encouraging to note that INDO-PSDCI theory correctly assigns the level ordering. The calculations predict a high degree of interstate mixing of both one-photon and two-photon character, and the extent of mixing calculated indicates that the observed separation in the FC maxima will invariably underestimate the actual level splitting. The calculations predict the interstate splitting to be $\sim$5000 cm^{-1}.

ATRSBS. Molecular orbital calculations predict two equilibrium positions for the perchlorate counterion in ATRSBS. These

(31) Twarowski, A. J.; Kliger, D. S. *Chem. Phys.* **1977**, *20*, 253.

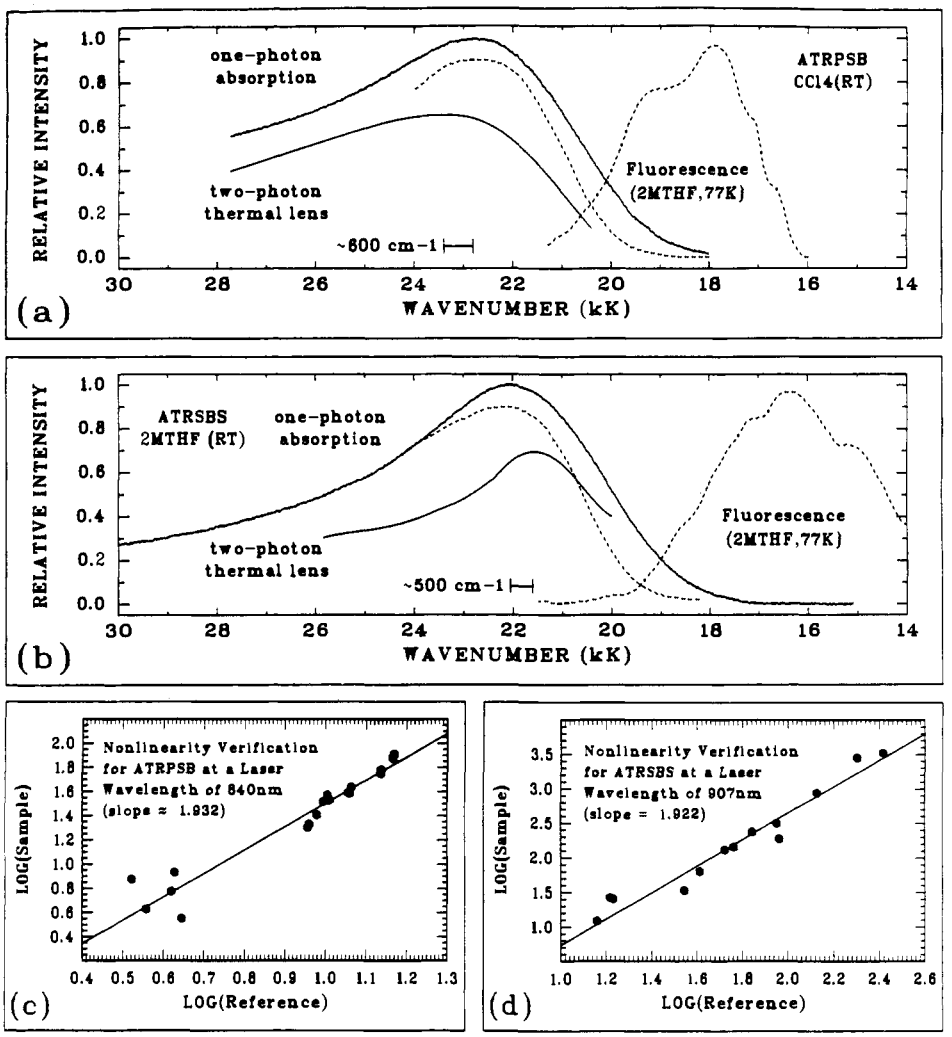

Figure 4. Comparison of the two-photon thermal lens spectra with the one-photon absorption and one-photon induced fluorescence spectra of ATRPSB (a) and ATRSBS (b) in nonpolar solvent environment. The two-photon spectra were obtained by using linearly polarized laser excitation and are plotted as a function of the combined energy of the two photons. Verification of the two-photon character for both spectra is demonstrated for selected wavelengths near the two-photon maxima in graphs (c and d). It was necessary to collect the two-photon thermal lens spectra of these two compounds by using different solvent environments (see text). For comparison, the dashed lines show the one-photon absorption and one-photon induced fluorescence spectra in 2M THF (77 K) glasses.

two positions are shown in Figure 5 (parts b and c), and the potential surface associated with symmetric approach of the counterions to the polyene are shown in Figure 7. Although the calculations predict that the counterion shown in Figure 5c is energetically more stable than the counterion position shown in Figure 5b, our neglect of solvent and our use of a semiempirical molecular orbital theory that underestimates nonbonding distances prevents a definitive assignment of one location vs. the other. Indeed, as shown in Figure 7, solvent tends to preferentialy stabilize the counterion configuration shown in Figure 5b, and at more "realistic" counterion separations, the latter configuration actually drops lower in energy. On the basis of these results, we postulate that these two structures will both be populated at ambient temperatures. The calculations also indicate that approach from the "top" vs. the "bottom" of the polyene chain is energetically equivalent (within calculational error). The "top" approach is shown in Figure 5 (parts b and c) for convenience only. A number of other possibilities were investigated by using INDO molecular orbital theory, but all other positions yielded energies greater than the two positions described above by at least 0.6 Hartrees (1 Hartree = 27.21 eV = 627.5 kcal mol^{-1}). This energy difference is sufficiently large to overwhelm continuum solvent effects and is also large enough to be outside of the error range expected for the semiempirical INDO molecular orbital theory. It is surprising, however, that interaction of the perchlorate counterion with one or more of the hydrogen atoms of the polyene system is not energetically competitive. Note that the primary interaction of the counterion in ATRPSB involves a hydrogen bond with the imine hydrogen (see Figure 5a). The salient difference between ATRSBS and ATRPSB, however, is the loss of the imine hydrogen atom and its replacement with a carbon–nitrogen bond associated with the five-membered pyrrolidiniminium ring. The charge on the imine proton in ATRPSB is calculated to be +0.174 (no counterion) (Table II). Although other atoms have larger positive charges than that calculated for the imine proton (see Table II), the additional stabilization associated with the formation of a hydrogen bond directs the counterion in ATRPSB to be localized as shown in Figure 5a. In contrast, no proton in ATRSBS has a charge larger than 0.061 (proton attached to C(14), Table II). This decreases the electrostatic component of the counterion–proton interaction significantly and diminishes the energetic stabilization associated with proton participation in counterion interaction. In contrast, carbon atoms 15 and 13 have large positive charges (0.308 and 0.247, respectively). It is, therefore, not surprising that the two most stable counterion conformations calculated involve strong interactions between the counterion oxygen atom and C(15). The NMR experiments provide further support for the counterion locations shown in Figure 5 (parts b and c) and suggest that these two conformations are in rapid exchange (NMR time scale) (see section IV.D.).

The effect of counterion location on level ordering and transition energies in ATRSBS is examined theoretically in Figure 6. The calculations indicate that both counterion locations produce a lowest lying $^1Ag^{*-}$-like state in agreement with the two-photon

Table II. Calculated Atomic Charges for ATRSBS and ATRPSB[a]

	ATRPSB no CI		ATRPSB Figure 5a		ATRSBS no CI		ATRSBS Figure 5b		ATRSBS Figure 5c	
atom	C	H	C	H	C	H	C	H	C	H
C(1)	48		45		48		45		45	
C(2)	−35	23	−32	18	−35	23	−32	19	−32	18
C(3)	−10	20	−9	15	−10	20	−10	15	−9	15
C(4)	−15	11	−14	7	−15	11	−14	7	−14	7
C(5)	34		15		33		14		16	
C(6)	−54		−37		−53		−36		−38	
C(7)	82	16	31	12	79	16	34	13	33	13
C(8)	−104	31	−65	23	−102	30	−67	22	−66	22
C(9)	153		83		149		89		91	
C(10)	−142	33	−87	26	−140	32	−91	23	−91	24
C(11)	157	13	73	9	153	13	83	12	99	15
C(12)	−163	46	−100	43	−161	45	−107	36	−106	38
C(13)	252		174		247		195		270	
C(14)	−221	61	−176	86	−220	61	−176	59	−201	55
C(15)	325	46	309	19	308	41	348	40	354	40
N	−174	174	−189	233	−131		−100		−142	
C(1′)	86	28	93	9	86	28	61	45	92	24
C(2′)	−12	20	−12	36	−11	32	−2	20	−12	21
C(3′)	5	11	2	0	−14	31	−4	20	−14	21
C(4′)	−26	18	−26	11	94	28	66	45	98	28
Cm(16)	−25	8	−23	6	−25	8	−23	6	−23	6
Cm(17)	−38	11	−38	10	−38	11	−38	10	−38	9
Cm(18)	−37	17	−34	15	−37	16	−34	14	−34	16
Cm(19)	−47	29	−35	18	−47	28	−36	19	−36	20
Cm(20)	−65	45	−50	30	−64	45	−53	35	−63	42
	none[b]		−788[b]		none[b]		−915[b]		−932[b]	
	1000[c]		0[c]		1000[c]		0[c]		0[c]	

[a] Calculated by using INDO-SCF-MO theory (see text). Charges for carbon atoms are listed under columns marked 'C' and hydrogen atom charges are listed under columns marked 'H'. All of the charges have been multiplied by 1000 for convenience, and if more than one hydrogen is attached to a given carbon atom, the hydrogen charges have been averaged. The charge listed for the anion is the net charge for the total counterion system. The total system charge is shown in the last row. [b] Anion. [c] Net Q.

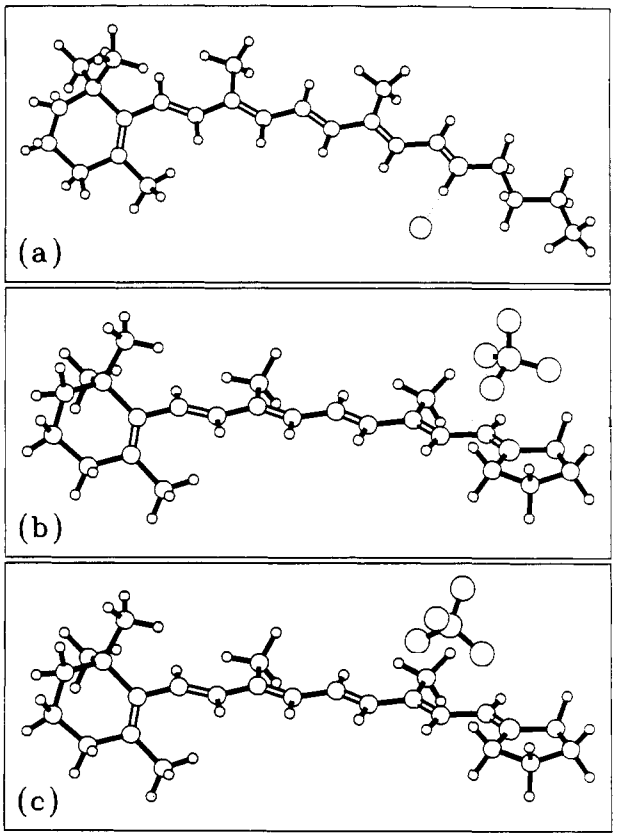

Figure 5. Assigned locations for the counterions in ATRPSB (a) and in ATRSBS (b and c). The spectroscopic and theoretical results indicate that the counterion (Cl^-) of ATRPSB forms a strong hydrogen bond with the amine proton (a). The spectroscopic and theoretical results for ATRSBS indicate that the counterion is in rapid exchange between two metastable environments as shown in inserts (b and c).

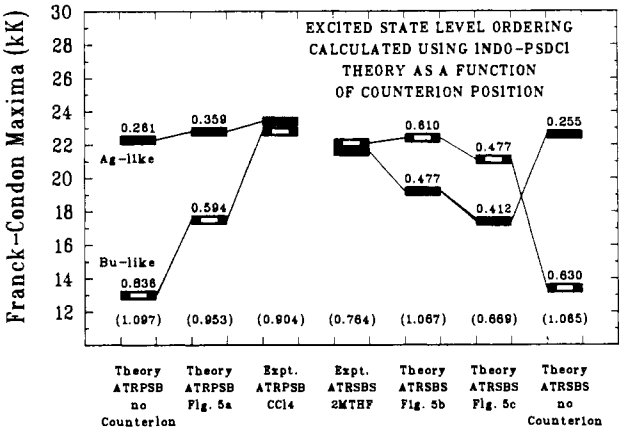

Figure 6. Comparison of theoretical and experimental results for the level ordering and one-photon oscillator strengths for ATRPSB (left three columns) and ATRSBS (right four columns). The theoretical calculations (based on INDO-PSDCI molecular orbital theory) were carried out for a positively charged retinyl polyene in the absence of a counterion (columns at extreme left and extreme right) and for the counterion environments shown in Figure 5. The experimental results are shown in columns 3 and 4, but strong mixing between the $^1A_g{}^{*-}$-like (solid rectangles) and $^1B_u{}^{*+}$-like (open rectangles) $\pi\pi^*$ excited states will shift the observed Franck–Condon maxima toward level separations which are smaller than the separations of the individual excited states. As noted in Section IV.C, the actual state splittings are >1500 cm^{-1}. Both theory and experiment support the assignment of a lowest lying $^1B_u{}^{*+}$-like state in ATRPSB and a lowest lying $^1A_g{}^{*-}$-like state in ATRSBS. The sum of the oscillator strengths for the two lowest lying $\pi\pi^*$ states are indicated in parentheses at the bottom of each column (the experimental number was obtained by integrating the λ_{max} absorption band).

studies. The experimental oscillator strength for the one-photon absorption band encompassing both the $^1A_g{}^{*-}$-like and $^1B_u{}^{*+}$-like states is 0.76. Both calculations overestimate the experimental oscillator strength but suggest that, based on oscillator strength

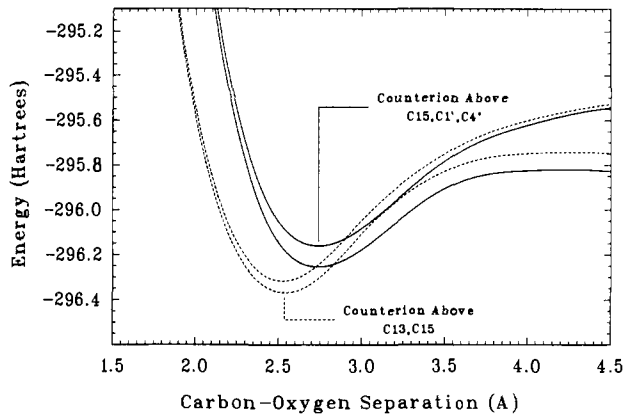

Figure 7. Theoretical (INDO-SCF-MO) prediction of the total energy of ATRSBS as a function of counterion location. The solid curves represent the energy of the counterion environment shown in Figure 5b as a function of the carbon–oxygen separation indicated by dotted lines in Figure 5b. The calculations assume arbitrarily that all three distances (dotted lines, Figure 5b) are identical. The upper solid curve was calculated assuming a vacuum environment, and the bottom curve was calculated for a highly polar, non-hydrogen bonding solvent with a dielectric constant of 150 (see text). The dashed potential surfaces were calculated in an analogous fashion for the counterion environment shown in Figure 5c for vacuum (top curve) and polar solvent (bottom curve).

criteria, the counterion location shown in Figure 5c dominates. In contrast, however, the transition energies match experiment more accurately for the counterion position shown in Figure 5b. The INDO-PSDCI calculations, therefore, provide little insight into which counterion location is more highly populated.

It is encouraging to note that our molecular orbital procedures predict correctly the experimental level orderings in ATRPSB and ATRSBS, particularly given the subtleties associated with a level ordering reversal within nearly homologous electronic environments (note similarity in charge distribution along polyene chain (Table II)). This is an important observation since molecular orbital theory played an important role in analyzing the two-photon data obtained for rhodopsin.[18] The success of our theoretical methods provides support for the binding site geometry assignment presented in ref 18.

C. Assignment of Excited State Level Ordering. An examination of the relationship between observed Franck-Condon maxima and excited state (system origin) level ordering is critical to an analysis of the data presented in this manuscript. The Franck–Condon distribution associated with excitation into, and/or fluorescence from, $^1A_g{}^{*-}$-like states is characteristically broader than that observed for the corresponding transition involving $^1B_u{}^{*+}$–like states (for excellent examples, see spectra in ref 22). This observation is in keeping with larger changes in geometry upon excitation into "covalent" $^1A_g{}^{*-}$-like vs. "ionic" $^1B_u{}^{*+}$-like states (see ref 3 and 15). The spectroscopic consequences of the above observation for inhomogeneously broadened absorption (or excitation) bands is that the energy separating the Franck–Condon maximum and the lower energy (obscured) system origin will be greater for $^1A_g{}^{*-}$-like $\leftarrow S_0$ absorption bands than for $^1B_u{}^{*+}$-like $\leftarrow S_0$ absorption bands. Thus, a $^1A_g{}^{*-}$-like state two-photon maximum below a $^1B_u{}^{*+}$-like state one-photon maximum will invariably herald $\Delta E(^1B_u{}^{*+}) > \Delta E(^1A_g{}^{*-})$ system origin level ordering. The converse cannot be assumed. The observation of a $^1A_g{}^{*-}$-like two-photon maximum $\sim$600 cm^{-1} above the $^1B_u{}^{*+}$-like one-photon maximum cannot, by itself, be interpreted to indicate a lowest lying $^1B_u{}^{*+}$-like state in ATRPSB. The following spectroscopic results provide strong evidence to support the assignment of a lowest lying $^1B_u{}^{*+}$-like state in ATRPSB.

Two-Photon Analysis. The two-photon excitation spectrum of ATRPSB was collected over a 7000-cm^{-1} range. Although the data do not extend to zero absorptivity at the red edge (see Figure 4a), the data are sufficient to extrapolate to red-edge behavior by using a least-squares fit of the two-photon absorptivity data to a log-normal curve (see, for example, ref 16). Normalization of the one-photon and two-photon data indicate that the red edges remain separated by >300 cm^{-1} at $\bar{\nu} >$ 18 000, with the two-photon distribution always above the one-photon distribution. If the system origin of the more two-photon allowed $^1A_g{}^{*-}$-like state were below the system origin of the more one-photon allowed $^1B_u{}^{*+}$–like state, these curves would cross between 18 000–21 000 cm^{-1} provided the system origin of the $^1A_g{}^{*-}$-like state has a relative two-photon Franck–Condon activity, I_{rel}, of >0.1. Since the $^1A_g{}^{*-}$-like system origin is electronically allowed under two-photon selection rules (ref 15) and should have a FC activity very similar to that observed in the vibronically resolved fluorescence spectrum of the model polyene Schiff base *N*-(2,4,6,8,10-dodecapentaenylidene)butylamine recorded by Palmer et al. (Figure 2 of ref 22; I_{rel} = 0.4), the above criterion is satisfied.

Fits of the one-photon and two-photon profiles using a sum of two Gaussians or log-normals indicates that the state separation is significantly larger than the separation in Franck–Condon maxima. If we use the INDO-PSDCI calculated mixing ratio of $\sim$0.6, we predict a state separation of >2250 cm^{-1} in ATRSBS ($^1A_g{}^{*-}$-like lowest) and a state separation of >2380 cm^{-1} in ATRPSB ($^1B_u{}^{*+}$-like lowest). The INDO–PSDCI calculations predict state splittings of $\sim$3500 cm^{-1} (ATRSBS) and $\sim$5300 cm^{-1} (ATRPSB). Although the simulations and molecular orbital calculations cannot be relied upon to provide rigorously accurate splittings, it is safe to conclude that the actual state splittings are >1500 cm^{-1}.

One-Photon Analysis. The fluorescence spectra of ATRPSB and ATRSBS are markedly different with respect to bandwidth and overlap with the one-photon absorption spectra. The full-width-at-half maximum (FWHM) of the ATRSBS fluorescence spectrum in 2M THF (77 K) is $\sim$4100 cm^{-1}. This value is similar to the fluorescence FWHM values observed for ATR and ATRSB in 3-methylpentane at 77 K ($\sim$4300 cm^{-1}). The latter two retinyl polyenes both have lowest lying $^1A_g{}^{*-}$-like states.[16,17] In contrast, the fluorescence spectrum of ATRPSB exhibits a FWHM of $\sim$3100 cm^{-1}. This difference is consistent with a smaller change in geometry on excitation into the lowest lying (fluorescing) state of ATRPSB vs. ATRSBS. Second, the normalized overlap of the fluorescence spectrum and the one-photon absorption spectrum is significantly larger for ATRPSB relative to that observed for ATRSBS, ATRSB, and ATR (last column of Table I).

Third, the fluorescence and one-photon Franck–Condon maxima separation is 4800 cm^{-1} in ATRPSB, a value similar to the fluorescence and two-photon FC maxima separation observed in ATR ($\sim$4700 cm^{-1}), ATRSB ($\sim$5200 cm^{-1}), and ATRSBS ($\sim$5000 cm^{-1}) (columns 7 and 8 of Table I). The above three observations indicate that the lowest-lying (fluorescing) state of ATRPSB is responsible primarily for the one-photon λ_{max} absorption band.

The one-photon and two-photon data are consistent with our principal conclusion; namely, ATRPSB has a lowest lying $^1B_u{}^{*+}$-like state and ATRSBS has a lowest lying $^1Ag^{*-}$-like state. The principal goal of the remaining discussion in this paper is to explain the molecular origins of this level ordering reversal. Assignment of counterion location is a key component of this analysis, and the following section is devoted to this goal.

D. NMR Spectroscopy. The ^{13}C and ^1H NMR spectra of ATRSBS and ATRSB are shown in Figures 8 and 9, and the assignments are given in Tables III and IV. The spectra have general similarities to those of related compounds studied previously.[27-29,36-39] The ^{13}C NMR spectrum of ATRSBS does not

(32) Fang, H. L.; Swofford, R. L. In *Ultrasensitive Laser Spectroscopy*, Kliger, D. S. Ed.; Academic Press: New York, 1983; pp 175–232.
(33) Birge, R. R.; Berge, C. T.; Noble, L. L.; Neuman, R. C. *J. Am. Chem. Soc.* **1979**, *101*, 5162.
(34) (a) Masthay, M. B.; Findsen, L. A.; Pierce, B. M.; Bocian, D. F.; Lindsey, J. S.; Birge, R. R. *J. Chem. Phys.* **1986**, *84*, 3901. (b) Birge, R. R. "Introduction to Two-Photon Spectroscopy" *In Spectroscopy of Biological Molecules*; Sandorfy, C., Theophanides, T., Eds.; Reidel: Boston, 1984; pp 457–471.
(35) Das, P. K.; Kogan, G.; Becker, R. S. *Photochem. Photobiol.* **1979**, *30*, 680.

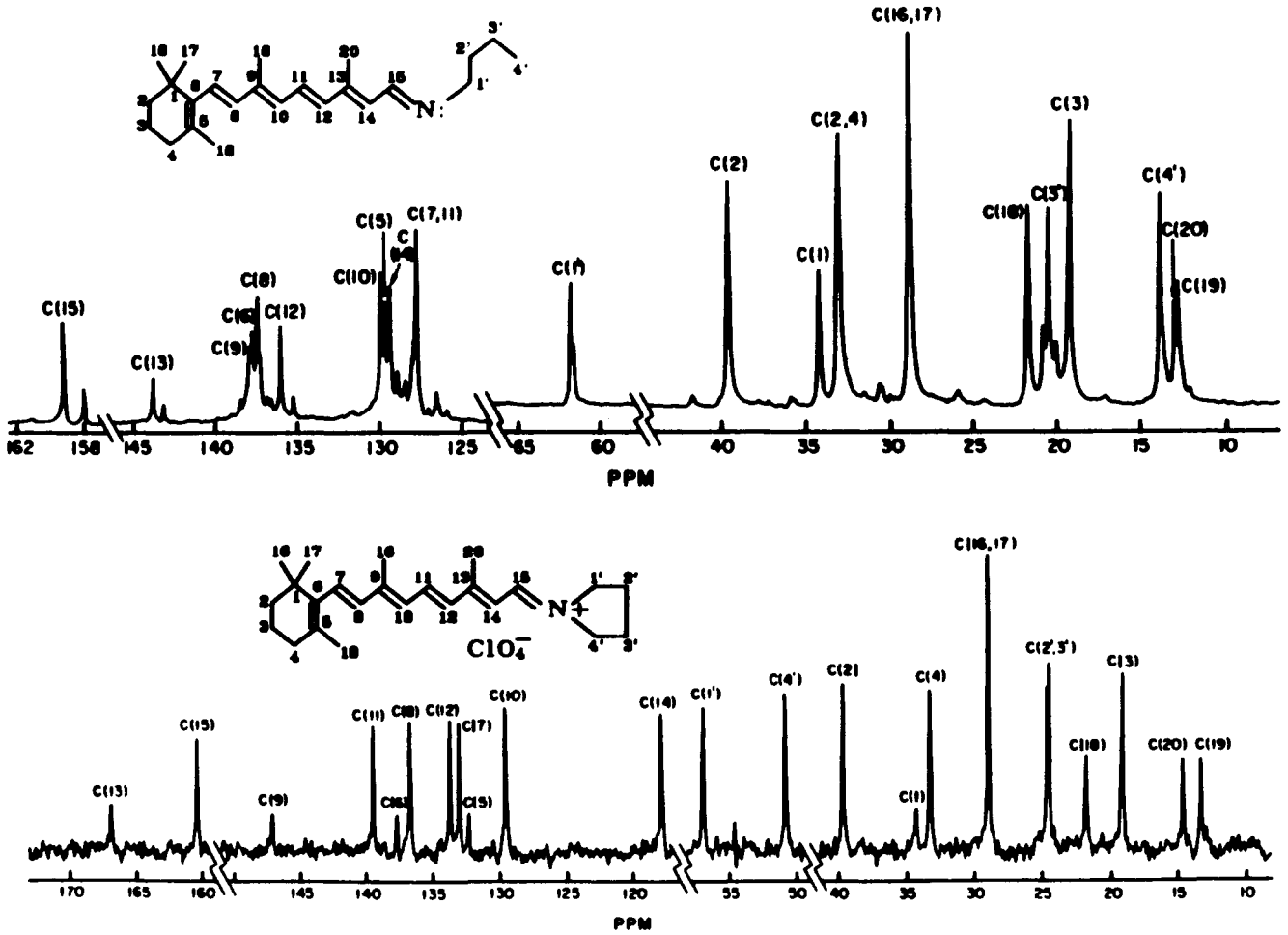

Figure 8. ^{13}C NMR spectra of ATRSBS and ATRSB in $CDCl_3$ at 25 °C. Assignments to the individual carbon atoms are shown above the individual resonances.

Table III. Natural Abundance ^{13}C NMR Spectra[c]

	ATRSBS chem shift,[a] ppm		ATRSB chem shift,[a] ppm
assignments	Me_2SO-d_6	$CDCl_3$	$CDCl_3$
C(1)	33.80	34.37	34.26
C(2)	*b*	39.75	39.67
C(3)	18.57	19.16	19.26
C(4)	32.66	33.40	33.11
C(5)	130.87	132.28	129.69
C(6)	137.13	132.62	137.74
C(7)	130.87	132.99	127.75
C(8)	136.42	136.64	137.42
C(9)	144.93	147.17	137.89
C(10)	129.82	129.55	129.94
C(11)	137.96	139.42	127.75
C(12)	133.91	133.68	136.02
C(13)	163.94	166.98	143.82
C(14)	118.93	117.92	129.40
C(15)	160.09	160.40	159.23
C(16,17)	28.71	29.04	28.96
C(18)	21.43	21.86	21.70
C(19)	12.85	13.37	12.81
C(20)	14.00	14.65	13.02
C(1′)	56.23	57.01	61.80
C(2′)	23.92	24.57	33.11
C(3′)	23.92	24.69	20.49
C(4′)	50.58	50.79	13.89

[a] ppm shift relative to $(Me)_4Si$ at 25 °C. [b] Obscured by solvent (Me_2SO) resonance. [c] At 125.767 MHz.

show evidence of single or double bond isomeric impurities (Figure 8a). The spectrum of ATRSB (Figure 8b), in contrast, shows the presence of minor impurities with ^{13}C peaks tentatively assigned to a small population of protonated species (e.g., peaks at 143 and 158 ppm, tentatively assigned to C(9) and C(13) of the protonated species).

Table IV. ^1H NMR Chemical Shifts of ATRSBS in Different Solvents[b]

assignments	Me_2SO-d_6	$CDCl_3$
2 H-C(2)	1.43	1.48
2 H-C(3)	1.56	1.63
2 H-C(4)	2.01	2.03
H-C(7)	6.45	6.52
H-C(8)	6.28	6.24
H-C(10)	6.39	6.27
H-C(11)	7.50	7.43
H-C(12)	6.68	6.56
H-C(14)	6.53	6.26
H-C(15)	8.96	8.85
3 H-C(16,17)	1.02	1.05
3 H-C(18)	1.69	1.79
3 H-C(19)	2.08	2.09
3 H-C(20)	2.33	2.42
2 H-C(1′)	3.85[a]	3.85[a]
2 H-C(2′)	2.04[a]	2.22[a]
2 H-C(3′)	1.97[a]	2.13[a]
2 H-C(4′)	4.00[a]	4.23[a]

[a] These assignments are tentative because the possibility that 2 H-C(4′) and 2 H-C(1′) as well as 2 H-C(3′) and 2 H-C(2′) are reversed cannot be excluded. [b] At 25 °C.

(36) Rowan, III, R.; Sykes, B. D. *J. Am. Chem. Soc.* **1974**, *96*, 7000.
(37) Becker, R. S.; Berger, S.; Dalling, D. K.; Grant, D. M.; Pugmire, R. J. *J. Am. Chem. Soc.* **1974**, *96*, 7008.
(38) Inoue, Y.; Tokito, Y.; Chujo, R.; Miyoshi, Y. *J. Am. Chem. Soc.* **1977**, *99*, 5592.
(39) Rabiller, C.; Danho, D. *Helv. Chim. Acta* **1984**, *67*, 1254.

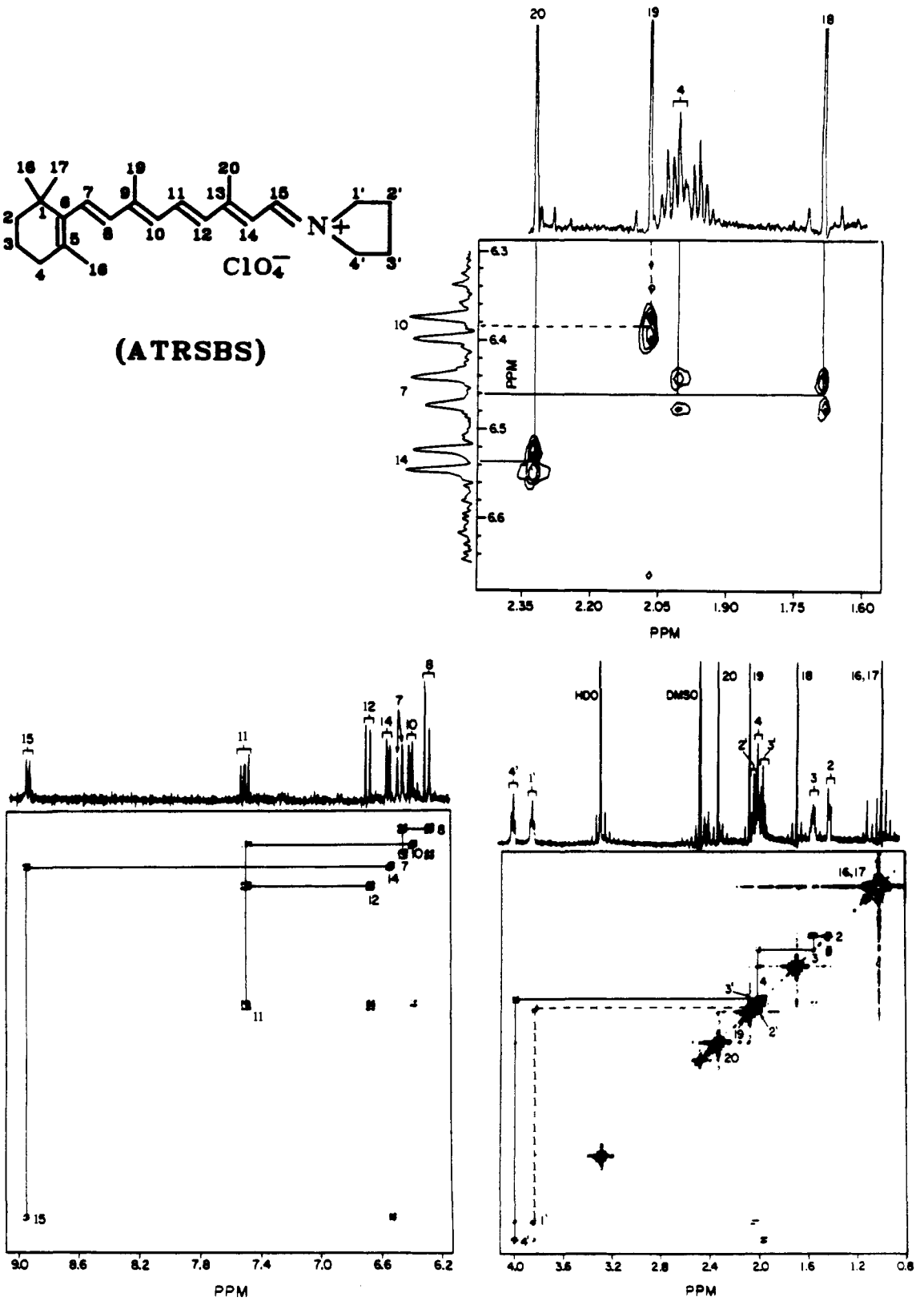

Figure 9. One-dimensional and two-dimensional (COSY) ^{1}H NMR spectra of ATRSBS in Me_2SO-d_6 at 25 °C. Proton assignments are indicated. (See text for details).

It was shown by Shriver et al.[28] by using semiempirical MO theory and the Pople–Karplus equation[40] that atomic electron densities are the most important contributors to the ^{13}C chemical shift differences of the polyene carbons. Therefore, we can in most cases narrow the discussion of the ^{13}C chemical shifts to consideration of the changes in the atomic charges on the corresponding carbon atoms as a function of molecule (see, for example, Figure 10). The major diagnostic feature of the formation of the Schiff base is seen in the chemical shift of C(15), which is shifted approximately 30 ppm upfield relative to ATR. Furthermore, the formation of the unprotonated Schiff base results in the upfield shift of the odd-numbered polyene carbons relative to ATR. This effect is caused by the substitution of the oxygen atom by the less

(40) Karplus, M.; Pople, J. A. *J. Chem. Phys.* **1963**, *38*, 2803.

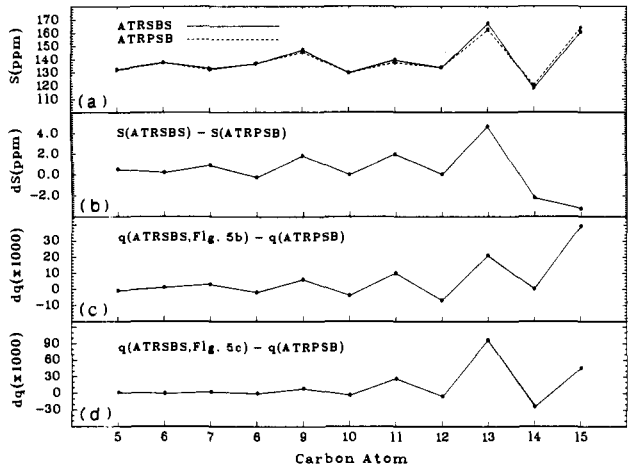

Figure 10. Theoretical analysis of ^{13}C chemical shifts in ATRSBS vs. ATRPSB: (a) plot of ^{13}C chemical shifts of ATRSB (this work) and ATRPSB (data from ref 27 and 28); (b) ^{13}C chemical shift differences between ATRSBS and ATRPSB. Positive values indicate downfield shift of ATRSBS relative to ATRPSB; and (c and d) relative shifts of ATRSBS and ATRPSB in terms of the relative charge distributions on the carbon atoms calculated by using INDO-SCF-MO molecular orbital theory for the two counterion positions shown in Figure (parts b and c).

electronegative nitrogen atom, with resulting release of electron density into the polyene chain. The formation of the iminium Schiff base salt or protonation of the Schiff base is accompanied by the delocalization of the formal positive charge on the nitrogen atom into the polyene chain, and the resulting decrease of the π-electron density is seen in the downfield shift of the odd-numbered polyene carbons of ATRSBS relative to ATRSB (Table III). The ^{13}C chemical shifts also provide information on the molecular geometry of the compounds studied. The shifts of carbons C(16)–C(18) show little change between ATRSBS and ATRSB (Table III) and are very close to the reported chemical shifts for similar compounds.[28] This indicates that there are no significant differences among these compounds in the torsional angle about the 6–7 single bond, which was shown previously to be a distorted 6-s-cis in solution.[36]

Our data, together with those of Shriver et al.[28] and Rabiller and Danho[39] and in conjunction with the resonance theory of the charge and bond order distribution within the polyene chain of similar compounds,[41] allow assignment of the position of the counterion in ATRSBS. Navangul and Blatz[41] showed that the close proximity of the counterion to the nitrogen atom results in the latter bearing a formal +1 charge, which in such a case is engaged in ionic interaction with the anion. (We use the term "formal" because the nitrogen atom is actually negative, and the positive charge is localized primarily on C_{13} and C_{15}, see Table II). The resonance theory predicts that the receding of the counterion causes increased delocalization of this positive charge into the polyene chain and the decrease of the electron densities on odd-numbered carbons, with much smaller changes in the electron densities of the even carbons (see Table II and ref 41), producing downfield shifts of the ^{13}C NMR resonances of the odd-numbered carbons. The plot of differences between ^{13}C chemical shifts of polyene carbons of ATRSBS and other related compounds shows that the odd-numbered carbons C(5, 7, 9, 11, 13) of ATRSBS are shifted downfield even relative to the protonated Schiff base, ATRPSB, indicating partial recession of the counterion in ATRSBS and reflecting a higher degree of dissociation of this molecule (Figure 10). The effect should be most pronounced near the place of perturbation, and indeed the largest polyene carbon differences are observed in the chemical shift of C(13) and the smallest in C(5). The notable exception is the behavior of the ^{13}C chemical shifts of C(15), which in ATRSBS is shifted little relative to ATRSB and displays a small (−3.25 ppm) upfield shift relative to ATRPSB (Table III). The behavior of the C(15) shift may be different because the deshielding induced on the nitrogen atom by the residual positive charge may be balanced by the decrease in double bond character and thus anisotropy of the C=N bond.

It is noteworthy, that the ^{13}C peaks of the odd-numbered carbons of ATRSBS shift upfield in Me_2SO-d_6 relative to $CDCl_3$ (Table III), while both the direct effect of the larger dielectric constant of Me_2SO and the resulting receding of the counterion should produce the opposite effect.[42] It has been suggested previously that the interaction of solvent molecules with a protonated Schiff base can produce the same quantitative effect as a formally charged anion.[41] Thus, the observed upfield shifts indicate an interaction of Me_2SO with ATRSBS which localizes the positive charge closer to the nitrogen atom. In other words, the principal solvent effect associated with Me_2SO is to replace the ClO_4^- counterion with a solvent cage which enhances stabilization of the positive charge in the C(13)···C(15) region. This result is contrary to that expected for a high dielectric "leveling solvent" (see ref 41) and deserves further study.

A comparison of the ^{13}C chemical shifts of the polyene carbons of ATRSBS and ATRPSB is presented in Figure 10. This comparison should provide insight into the location of the counterion in ATRSBS since the counterion location in ATRPSB is known. The previous studies by Shriver et al.[28] have provided support for the view that atomic charge is a dominant contributor to differences in ^{13}C chemical shift in polar polyenes. In general, deshielding the carbon nucleus by decreasing electron density will cause a downfield shift of the ^{13}C resonance [a downfield shift (decreased h_0) produces an increased chemical shift (σ (ppm))]. Conversely, more negative carbon atoms have shielded nuclei resulting in upfield (smaller σ (ppm)) shifts. These qualitative statements follow from the Pople–Karplus equation which predicts (all other factors remaining constant) that the chemical shift, σ^{AA}, is proportional to $[3.25 + 0.35\, q_a]^3$, where q_a is the charge on atom A.[40] We compared experimentally observed changes of ^{13}C chemical shifts between ATRPSB and ATRSBS with calculated differences of the charge distributions between the corresponding carbon atoms (Figure 10). The two alternative counterion environments used for calculations are shown in Figure 5 (parts b and c). Based on the above arguments, there should be a positive correlation between these two parameters if our counterion assignments are correct. Analysis of Figure 10 suggests that the counterion location shown in Figure 5c is slightly more successful than that shown in Figure 5b in terms of accommodating the chemical shift data. However, a linear combination of both assignments leads to the best agreement with experiment. The ^{13}C chemical shift data support our theoretical prediction that there are two viable counterion locations (Figure 5 (parts b and c)), and indicate that these two are in a fast dynamic equilibrium on the NMR time scale ($\ll 50$ μs).

The ^1H NMR spectra of ATRSBS in Me_2SO-d_6 are shown in Figure 9, and the peak positions are listed in Table IV. The two-dimensional spectra show clearly all of the connectivities associated with the ^1H–^1H vicinal couplings (Figure 9). In addition, we detected five long-range couplings, four of which involve the protons of the polyene chain: ^4J(H–C(10), $H_3C(19)$), ^4J(H–C(14), $H_3C(20)$), ^5J(H–C(7), H-C(4)), and ^5J(H–C(7), $H_3C(18)$) (Figure 9). These couplings were also detected in ATR by using 2-D spin-echo correlation spectroscopy[43] and corresponding to the largest long-range coupling constants found in this molecule.[44,45] A fifth long-range coupling observed by us corresponds to ^4J($H_2C(1')$, $H_2C(4')$) (Figure 9).

Both the one- and two-dimensional spectra are similar to previously reported spectra of related compounds.[29,39,43–46] In

(41) Navangul, H. V.; Blatz, P. E. *J. Am. Chem. Soc.* **1978**, *100*, 4340.

(42) Sakurai, M.; Ando, I.; Inoue, Y.; Chujo, R. *Photochem. Photobiol.* **1981**, *34*, 367.

(43) Wernly, J.; Lauterwein, J. *Helv. Chim. Acta* **1983**, *66*, 1576.

(44) Honig, B.; Hudson, B.; Sykes, B. D.; Karplus, M. *Proc. Natl. Acad. Sci. U.S.A.* **1971**, *68*, 1289.

(45) Rowan, III, R.; Warshel, A.; Sykes, B. D.; Karplus, M. *Biochemistry* **1974**, *13*, 970.

the scope of this work, it is important to consider the chemical shifts and vicinal coupling constants of the polyene protons, especially near the nitrogen atom. If one of these protons were engaged in the formation of a hydrogen bond, one would expect to observe a noticeable downfield shift of the corresponding resonance. Comparison of our data with previous studies[27,29,39] shows the absence of such a shift for any proton in ATRSBS and indicates that no polyene proton is forming a hydrogen bond with the counterion. The data do leave open the possibility of weak hydrogen bonds formed between the counterion oxygen atoms and the protons attached to C(1′) and C(4′). The chemical shifts of polyene protons from H–C(8) to H–C(15) move upfield upon the change of solvent from Me_2SO-d_6 to $CDCl_3$ (Table IV). The opposite effect would be expected if the counterion were located closer to the chromophore in $CDCl_3$. The upfield shift of these protons is similar to the solvent-dependent ^{13}C-NMR shift behavior of the corresponding carbons (Table III) and is consistent with strong electrostatic interaction of ATRSBS with Me_2SO.

The vicinal proton coupling constants H–C(7), H–C(8) (15.9 Hz), H-C(10), H-C(11) (11.7 Hz), and H–C(11), H–C(12) (15.0 Hz) are very close to those reported for ATR[27,36] indicating that an essentially planar, trans configuration of the polyene chain is maintained in ATRSBS.

E. Photophysical Properties of ATRSBS and ATRPSB. The above spectroscopic and theoretical results indicate that ATRPSB has a lowest lying $^1B_u{}^{*+}$-like state and that ATRSBS has a lowest lying $^1A_g{}^{*-}$-like state. The equilibrium counterion environments are shown in Figure 5, but it should be noted that the two counterion locations assigned for ATRSBS are in dynamic equilibrium on the NMR time scale with a higher population of Figure 5c than of Figure 5b counterions. The more diffuse counterion geometry associated with ATRSBS produces a more covalent environment than that associated with the highly localized hydrogen bonded counterion environment associated with ATRPSB. Accordingly, the protonated Schiff base exists in a more ionic environment than the Schiff base salt, and this leads to increased stabilization of the ionic "$^1B_u{}^{*+}$" state resulting in a level ordering reversal placing the ionic state below the covalent "$^1A_g{}^{*-}$" $\pi\pi^*$ excited state. These observations are fully consistent with the previous experimental and theoretical studies on Schiff bases and protonated Schiff bases.[3,15,17,18] Our results might appear to conflict with the previous spectroscopic studies of Palmer et al., which indicated that protonation of dodecapentaenylidene-*n*-butylamine Schiff base (DDPSB) did not induce a level ordering reversal.[22] In fact, our results are fully consistent with the spectroscopic observations of Palmer et al. These investigators studied DDPSB in a hydrocarbon solvent (PMH) by using a 5:1 ratio of perfluoro-*tert*-butyl alcohol/DDPSB to induce protonation. This complex provided a delocalized counterion which could be supported by a hydrocarbon solvent.[47] This system thus shares the "diffuse" features of the perchlorate counterion in ATRSBS. That both DDPSB and ATRSBS have lowest lying $^1A_g{}^{*-}$-like states supports the conclusions of the present study. One would expect from the above discussion, however, that DDPSB in the presence of excess HCl in EPA (77 K) would generate a situation analogous to ATRPSB. Both compounds should have lowest lying $^1B_u{}^{*+}$-like states. Unfortunately, the spectra of both compounds are inhomogeneously broadened preventing definitive assignments of the systems origins (e.g., Figure 3a above; Figure 6 of ref 22). Furthermore, in the highly polar environment afforded by EPA, the system origins of absorption and fluorescence are not expected to overlap. This is due to an increase in the dipole moment of a protonated Schiff base upon excitation ($\Delta\mu \simeq 12$ D, see ref 48) and the resultant increase in electrostatic stabilization accompanying solvent reorganization in the excited state prior to fluorescence. An approximate value for this shift has been derived by Lippert[49] and Mataga et al.[50] by using a spherical cavity reaction field model

$$(\Delta\tilde{\nu}_{i\leftarrow 0} - \Delta\tilde{\nu}_{i\rightarrow 0}) \cong \frac{2}{hc}\frac{(\mu_i - \mu_0)^2}{a^3}\left[\frac{(\epsilon - 1)}{(2\epsilon + 1)} - \frac{(n^2 - 1)}{(2n^2 + 1)}\right] \quad (1a)$$

$$\Delta\Delta\tilde{\nu}(\mathrm{cm}^{-1}) \simeq \frac{10064|\Delta\mu(\mathrm{D})|^2}{[a\ (\mathrm{A})]^3}\left[\frac{(\epsilon - 1)}{(2\epsilon + 1)} - \frac{(n^2 - 1)}{(2n^2 + 1)}\right] \quad (1b)$$

where μ_0 and μ_i are the ground and excited state dipole moments, respectively, a is the cavity radius, ϵ is the solvent dielectric constant, and n is the solvent refractive index. We assume that the solvation properties of EPA are determined primarily by the ethanol fraction for highly polar solutes since absorption maxima of retinyl polyenes in EPA and ethanol are similar. Assuming $\Delta\mu = 12$ D,[48] $a = 4.3$ Å, $\epsilon = 24.55$, and $n = 1.359$ we calculate $\Delta\Delta\tilde{\nu} = 5279$ cm^{-1}. The use of a spherical cavity approximation and uncertainty in the assignment of $\Delta\mu$, a, ϵ, and n relegates the above calculation to qualitative significance. Nonetheless, the fact that reasonable values yield a $\Delta\Delta\tilde{\nu}$ comparable to the observed separation of the first vibronic bands in absorption and fluorescence of DDPSB:HCl (EPA) ($\sim$3500 cm^{-1}, Figure 6, ref 22) suggests that this separation cannot be used as evidence for a lowest lying "forbidden" state. The separation of electronic origins of polar compounds in polar solvents can be due entirely to solvent-induced shifts associated with dipole moment changes upon excitation.

The above comments are not intended to suggest a disagreement between this study and that of Palmer et al.[22] These authors were careful to note that a conclusive assignment of level ordering for DDPSB:HCl in EPA was not possible due to ambiguity in system origin assignment. Our results suggest, however, that DDPSB:HCl has a lowest lying $^1B_u{}^{*+}$-like state based on the similarities between this compound and ATRPSB.

Becker and Freedman have argued recently that level mixing, rather than level ordering reversal, represents the key photophysical property responsible for efficient photoisomerization.[23] These authors suggested that their observations conflicted with the previous theoretical studies of Birge and Hubbard.[19,20] The conflict is largely semantic. Birge and Hubbard noted that mixing of the $^1A_g{}^{*-}$-like and $^1B_u{}^{*+}$-like states was responsible for the theoretical prediction of a low barrier to retinyl polyene 11-*cis* → 11-trans photoisomerization.[19] It was further noted in ref 19 that a lowest lying $^1B_u{}^{*+}$-like state enhances mixing and that the barrierless 11-cis → 11-trans dihedral surface in rhodopsin is due to three effects: (1) torsionally enhanced state mixing, (2) a lowest lying "$^1B_u{}^{*+}$"-like state, and (3) a fixed counterion. No experimental evidence was presented by Becker and Freedman to dispute the above theoretical predictions. The observation of high quantum yields for photoisomerization of 11-cis Schiff bases in highly polar solution ($\Phi = 0.34$, acetonitrile) is noteworthy and supports the hypothesis that excited state mixing enhances photoisomerization rates. However, the quantum yield of the primary photochemical event in rhodopsin is 0.67. The fact that the latter quantum yield is approximately twice as large as that measured for the Schiff base in solution tells only part of the story. The excited state of rhodopsin has an observed lifetime of less than 15 ps.[51] Retinyl Schiff bases have observed lifetimes of $\sim$6 ns.[35] Accordingly, the rate of photoisomerization in rhodopsin is $\sim$800 times larger than Schiff bases in solution. Analogous calculations based on the data of ref 13, 35, 52, and 53 indicate that 11-cis protonated Schiff bases photoisomerize with rates 2–40 times larger than

(46) Patel, D. J. *Nature (London)* **1969**, *221*, 825.
(47) We thank Professor R. L. Christensen for suggesting this explanation for the environmental origins of a lowest lying $^1A_g{}^{*-}$-like state in 5:1 mixtures of perfluoro-*tert*-butyl alcohol:DDPSB in PMH solvent.
(48) Mathies, R.; Stryer, L. *Proc. Natl. Acad. Sci. U.S.A.* **1976**, *73*, 2169.
(49) Lippert, E. *Z. Natursch., A: Astrophys., Phys., Phys. Chem.* **1955**, 10A, 541. Lippert, E. *Z. Elektrochem.* **1957**, *61*, 962.
(50) Mataga, N.; Kaifu, Y.; Koizumi, M. *Bull. Chem. Soc. Jpn.* **1955**, *28*, 690.
(51) Doukas, A. G.; Junnarkar, M. R.; Alfano, R. R.; Callender, R. H.; Balogh-Nair, V. *Biophys. J.* **1985**, *47*, 795.
(52) Huppert, D.; Rentzepis, P. M.; Kliger, D. S. *Photochem. Photobiol.* **1977**, *25*, 193.
(53) Freedman, K.; Becker, R. S.; Hannak, D.; Bayer, E. *Photochem. Photobiol.* **1986**, *43*, 291.

11-cis Schiff bases in solution (the value is highly solvent dependent). All of the data can be rationalized by using the theoretical models presented in ref 19–21.

Finally, it should be noted that solvent can play an important role in determining level ordering. Onsager reaction field calculations[33] based on solute properties predicted by using IND-O-PSDCI theory predict that the $^1B_u{}^{*+}$-like state in protonated Schiff bases and Schiff base salts will be stabilized preferentially by increasing solvent polarity, hydrogen bonding capability, or refractive index. It may be possible to invert the level ordering in ATRSBS by using highly polar and/or dispersive solvents. An attempt to induce level ordering reversal by using the mixed solvent, EPA, however, failed apparently to induce a lowest lying $^1B_u{}^{*+}$-like state (see Figure 3 and above discussion). Further studies in this area are needed to clarify the role of solvent and protein environment on excited state level ordering of solvated and protein bound retinyl Schiff base and protonated Schiff base polyenes.

Acknowledgment. This work was supported in part by grants to RRB from the National Institutes of Health (GM-34548) and the National Science Foundation (CHE-8518155). We gratefully acknowledge use of the Southern California Regional NMR Facility, which is funded by Grants CHE-7916324 and CHE-8440137 from the National Science Foundation. We thank Professor R. L. Christensen for interesting and helpful discussions.

Registry No. ATRSBS, 23369-82-6; ATRPSB, 61769-46-8; ATR, 116-31-4; ATRSB, 61769-47-9.

Reactivity and Intersystem Crossing of Singlet Methylene in Solution

Nicholas J. Turro,* Yuan Cha, and Ian R. Gould†

Contribution from the Department of Chemistry, Columbia University, New York, New York 10027. *Received September 2, 1986*

Abstract: Evidence is reported which demonstrates that singlet methylene, produced from the photolysis of diazomethane or diazirine, undergoes intersystem crossing to form triplet methylene in perfluorohexane solvent. The results of triplet sensitized photolysis and of direct photolysis experiments with dilute concentrations of substrate (*cis*- and *trans*-2-pentene and chloroform) appear to be essentially identical. Stern–Volmer analyses of the competition kinetics between acetonitrile and 2-pentenes or chloroform for singlet methylene are consistent with the near diffusion controlled reactivity of singlet methylene. With the assumption of diffusion-controlled reactions for singlet methylene, plots of the quantum yield for singlet vs. triplet reaction for methylene allow the first estimate ($\leq 8 \times 10^8$ s^{-1}) of the rate of intersystem crossing of singlet methylene in the condensed phase. This value is considerably smaller than the value that is extrapolated to the solution phase from results in the gas phase. The possible reasons for this difference are discussed.

Methylene (CH_2), the parent of the carbene family, has attracted the attention of organic chemists,[1] theorists,[2] spectroscopists,[3] and chemical physicists.[4,5] Almost all of the quantitative information concerning this species is derived from gas-phase investigations,[6] from which it has been concluded that CH_2 is a ground state triplet ($^3CH_2$) and that a low-lying singlet state ($^1CH_2$) exists at about 9 kcal/mol[7] above the ground state (Figure 1). Methylene possesses one carbon atom, two hydrogen atoms, and two nonbonding electrons. The two nonbonding electrons occupy the σ and π orbitals with their spins parallel for the more linear $^3CH_2$ ($\delta = 136°$), while they occupy the σ orbital paired spins for the lowest energy singlet methylene ($\theta = 102°$) (Figure 1). Both states have been observed spectroscopically in the gas phase,[3] and from kinetic investigations[4,5] it has been concluded that $^1CH_2$ is quenched by all additives, even inert gases, with high efficiency. Indeed, extrapolation of the gas-phase quenching data to the solution phase leads to the expectation that the lifetime of $^1CH_2$ will be of the order of picoseconds in the condensed phase. For example, $^1CH_2$ is quenched by He in the gas phase[4] with a rate constant of ca. 4×10^{-12} cm^3 molecule^{-1} s^{-1}, which translates into a bimolecular rate constant of ca. 2×10^9 M^{-1} s^{-1}. For an organic solvent concentration of 5 M, the rate of quenching for a completely inert solvent (such as helium!) would be 1×10^{10} s^{-1}, implying a lifetime of the order of 50 ps or less for $^1CH_2$ in solution. This expectation is based on the assumption that the rate of the $^1CH_2$ deactivation is a linear function of pressure even at high pressure (or in the solution phase). Since quenching must involve either reaction or intersystem crossing to $^3CH_2$, one is led to expect either the absence of the latter in solution upon direct production of $^1CH_2$ (in the case of reaction) or essentially immediate production of $^3CH_2$ (in the case of rapid intersystem crossing). Since distinct chemistries on $^1CH_2$ (direct photoexcitation of diazomethane)[8] and $^3CH_2$ (triplet sensitized excitation of diazomethane)[9] have been demonstrated in solution, *a "dilution effect" on the products of $^1CH_2$ is not expected from extrapolation of the gas-phase results because both intersystem crossing or reaction of this species are expected to occur at near collision controlled rates.* Indeed, the results in the literature[10] strongly support the thesis that $^1CH_2$ reacts with all substrates at the diffusion-controlled rate, since it is found to react with the CH bonds of even saturated hydrocarbons in a rather indiscriminate manner.[11] However, a qualitative investigation of the dilution

† Current address: Eastman Kodak Research Laboratories, Rochester, NY 14650.

(1) For a review see: Kirmse, W. *Carbene Chemistry*, 2nd ed.; Academic Press, Inc.: New York, 1971; Chapters 5–11.
(2) Harrison, J. F. *Acc. Chem. Res.* **1974**, *7*, 378 and references therein.
(3) Herzberg, G. *Proc. R. Soc. (London)* **1961**, *A262*, 291.
(4) Langford, A. O.; Petek, H.; Moor, C. B. *J. Chem. Phys.* **1983**, *78*, 6650 and references therein.
(5) Ashfold, M. N. R.; Fullstone, M. A.; Hancock, G.; Duxburg, G. *Mol. Phys.* **1982**, *45*, 887.
(6) Laufer, A. H. *Rev. Chem. Intermed.* **1981**, *4*, 225.
(7) Leopold, D. G.; Murray, K. K.; Miller, A. E. S.; Lineberg, W. C. *J. Chem. Phys.* **1984**, *83*, 4849 and references therein.
(8) Woodworth, R. C.; Skell, S. P. *J. Am. Chem. Soc.* **1959**, *81*, 3383.
(9) Kopecky, K. R.; Hammond, G. S.; Leermaker, P. A. *J. Am. Chem. Soc.* **1962**, *84*, 1015.
(10) Baron, w. J.; DeCamp, M. R.; Hendrick, M. E.; Jones, M., Jr.; Levin, R. H.; Sohn, M. B. In *Carbenes*; Jones, M., Jr., Moss, R. A., Eds.; Wiley: New York, 1973; Vol. I, pp 1–19.
(11) Doering, W. v. E.; Buttery, R. G.; Laughlin, R. G.; Chaudhuri, N. *J. Am. Chem. Soc.* **1956**, *78*, 3224.

0002-7863/87/1509-2101$01.50/0